Indonesian Journal of Modern Science and Technology Modern (IJMST)
Vol. 2, No. 1, January 2026, pp. 39-50
E-ISSN: 3090-3831 | DOI: doi.org/10.64021/ijmst.2.1.39-50.2026

Vibrational, Optical Band Gap, Urbach Energy, and Thermal Activation Analysis of $TiO_2/CaTiO_3$ Perovskite

Kormil Saputra [1,2], Dian Wijaya Kurniawidi [1,*], Aws M Aseer Nejres [3]
[1] Physics Study Program, University of Mataram, Mataram, Indonesia
[2] Center of Advanced Functional Material and Biosensor, Tinta Emas Institute, Mataram, Indonesia
[3] College of Pharmacy, University of Mosul, Iraq

ARTICLE INFO

Article history:

Received January 2, 2026
Revised January 15, 2026
Published January 21, 2026

Keywords:

$TiO_2/CaTiO_3$;
Band Gap Energy;
Urbach Energy;
Kubelka–Munk;

ABSTRACT (10 PT)

$TiO_2/CaTiO_3$ is an oxide perovskite with considerable potential for photocatalytic, optical-sensing, and semiconductor-based functional-material applications. This study aimed to evaluate the vibrational characteristics, optical properties, band gap energy, Urbach energy, and kinetic and activation thermodynamic parameters of $TiO_2/CaTiO_3$.. The material was characterized using FTIR, UV–Vis spectroscopy, Kubelka–Munk analysis, Tauc plots, and Differential Thermal Analysis (DTA). The FTIR results revealed characteristic absorption bands in the low-wavenumber region associated with Ti–O, Ti–O–Ti, and Ca–O–Ti vibrations, indicating the formation of the $TiO_2/CaTiO_3$ perovskite framework. The UV–Vis spectrum showed dominant absorption in the ultraviolet region with an extension toward the visible region. Kubelka–Munk analysis yielded direct and indirect band gap energies of 2.896 and 2.897 eV, respectively, whereas the Tauc-plot method produced values of 2.894 and 2.896 eV. The Urbach energies obtained using the Kubelka–Munk approach ranged from 0.173 to 0.189 eV, while the Tauc-plot approach yielded 0.449–0.686 eV. These differences demonstrate the sensitivity of the estimation method to the baseline and fitting region and indicate the presence of tail states associated with optical disorder. DTA analysis showed a peak temperature of 623.31 K, with Ea = 7.853 kJ mol-1, ΔH* = 1.511 kJ mol-1, ΔG* = 233.89 kJ mol-1, ΔS* = −301.26 J mol-1 K-1, and ln A = −5.238. Overall, TiO2/CaTiO3 exhibited vibrational, optical, and thermal characteristics that support its potential as an oxide-perovskite functional material.

Corresponding Author:

Dian Wijaya Kurniawidi, Physics Study Program, University of Mataram, Mataram, Indonesia
Email: diankurnia@unram.ac.id

1. INTRODUCTION

Authors

Calcium titanate ($CaTiO_3$) is an ABO_3-type oxide perovskite that has attracted considerable attention because of its chemical and thermal stability and its optical and electronic properties, which are relevant to functional-material applications. In recent years, $CaTiO_3$ has been investigated for photocatalysis, pollutant degradation, optoelectronic materials, sensors, and energy-related systems because it forms a stable crystal structure and exhibits the characteristic optical response of an oxide semiconductor. Cerón-Urbano et al.,

demonstrated the use of $CaTiO_3$ nanoparticles to degrade emerging contaminants, including methyl orange and levofloxacin, highlighting the material's potential for photocatalytic environmental remediation [1].

Although $CaTiO_3$ is known as a wide-band-gap oxide semiconductor, its optical properties are strongly influenced by the synthesis method, calcination temperature, particle size, crystal structure, lattice defects, and surface states. Mishra et al. showed that variations in calcination temperature affect the structural, optical, and photocatalytic characteristics of $CaTiO_3$ nanoparticles [2]. These findings confirm that the behavior of $TiO_2/CaTiO_3$ is determined not only by its chemical composition but also by processing conditions that can alter its local structure, crystallinity, and light-absorption response.

Vibrational characterization using Fourier Transform Infrared Spectroscopy (FTIR) is important for identifying the formation of characteristic metal–oxygen bonds in $TiO_2/CaTiO_3$. In titanate perovskites, Ti–O, Ti–O–Ti, and Ca–O–Ti vibrations can serve as preliminary indicators of the formation of a Ca–Ti–O framework. FTIR can also reveal surface species, including hydroxyl groups, adsorbed water, carbonates, and precursor residues remaining after synthesis. Consequently, FTIR analysis is required to determine whether the product has developed the oxide network associated with calcium titanate rather than remaining as a physical mixture of unreacted precursors. A recent investigation of a $TiO_2/CaTiO_3$ composite similarly combined FTIR with DTA-TG, XRD, SEM-EDS, BET, and UV–Vis measurements to assess the formation and stability of a $TiO_2/CaTiO_3$-based perovskite structure [3].

In addition to its vibrational structure, the optical properties of $TiO_2/CaTiO_3$ must be evaluated quantitatively using UV–Vis spectroscopy or diffuse reflectance spectroscopy. Optical band gap energy is commonly estimated using the Kubelka–Munk transformation and Tauc plots, particularly for powdered or reflective solid samples. However, band gap values obtained from reflectance data must be interpreted carefully because the Kubelka–Munk function depends on assumptions concerning scattering and absorption, while Tauc plots are sensitive to the baseline, the selected linear region, and the assumed optical transition. Landi et al. discussed the potential misuse of the Kubelka–Munk function when its underlying assumptions are not satisfied [4]. The limitations of conventional Tauc analysis and the influence of baseline absorption have also been demonstrated in recent studies [5], [6].

Urbach energy is another important optical parameter because it provides information on optical disorder and tail states near the band edge. It is associated with structural disorder, lattice defects, oxygen vacancies, local distortion, and surface states that broaden the optical response of a material. Therefore, the combined evaluation of band gap and Urbach energies provide a more comprehensive description of the relationship among local structure, optical defects, and light absorption in $TiO_2/CaTiO_3$ [7]. Thermal stability is also an important consideration. Differential Thermal Analysis (DTA) can identify major thermal events, including the release of surface species, thermal relaxation, decomposition of residual compounds, and minor structural transformations. The peak temperature obtained from a DTA curve can be used to calculate kinetic and activation thermodynamic parameters, such as activation energy, the pre-exponential factor, activation enthalpy, activation Gibbs free energy, and activation entropy. Nevertheless, parameters derived from thermal analysis should be interpreted as apparent kinetic parameters rather than as the thermodynamics of product formation [8].

Based on these considerations, an integrated analysis of FTIR, UV–Vis spectra, band gap energy, Urbach energy, and DTA is important for developing a comprehensive understanding of the vibrational characteristics, optical response, electronic disorder, and thermal stability of $TiO_2/CaTiO_3$. Accordingly, this study evaluated $TiO_2/CaTiO_3$ by identifying metal–oxygen vibrations using FTIR, analyzing its optical response using UV–Vis spectroscopy, determining the band gap and Urbach energies through Kubelka–Munk and Tauc-plot approaches, and evaluating its kinetic and activation thermodynamic parameters from DTA data. This integrated approach provides a basis for assessing the suitability of $TiO_2/CaTiO_3$ as an oxide-perovskite functional material.

2. METHODS

2.1. Research Design

This study is a continuation of the work reported by Kurniawidi et al. on the synthesis and characterization of $TiO_2/CaTiO_3$ composites derived from Pinctada maxima shell waste [3]. In the previous study, $TiO_2/CaTiO_3$ was synthesized by coprecipitation using shell-derived $CaCO_3$ as the calcium source and TiO_2 as the titanium source. Beyond the thermal event at 623.31 K, no significant DTA peak was detected up to the calcination temperature of 700 °C, suggesting that no major phase transformation or bulk lattice reconstruction occurred within this temperature range. Therefore, the event at 623.31 K is more reasonably attributed to the release of

surface species, such as adsorbed moisture, hydroxyl groups, or residual precursor species, while the $TiO_2/CaTiO_3$ structure remained thermally stable at higher temperatures. The present analysis focuses on the vibrational characteristics, optical properties, band gap energy, Urbach energy, and kinetic and activation thermodynamic parameters of $TiO_2/CaTiO_3$ based on FTIR, UV–Vis, and DTA data.

2.2. Preparation of the $TiO_2/CaTiO_3$ Sample

The $TiO_2/CaTiO_3$ composite analyzed in this study was synthesized through the coprecipitation method reported by Kurniawidi et al. [3]. A calcium precursor derived from Pinctada maxima shell waste and TiO_2 as the titanium source were mixed and homogenized, followed by precipitation, washing, drying, and calcination at 700 °C. Before characterization, the resulting $TiO_2/CaTiO_3$ composite was ground into a fine, homogeneous powder to minimize the influence of particle agglomeration on the FTIR, UV–Vis, and DTA measurements. The homogenized sample was subsequently used to evaluate its vibrational characteristics, optical properties, band gap energy, Urbach energy, and thermal stability.

2.3. FTIR Characterization

Fourier Transform Infrared Spectroscopy (FTIR) was used to identify the chemical bonds and vibrational modes present in the $TiO_2/CaTiO_3$ sample. The FTIR spectrum was recorded over the wavenumber range of 4000–400 cm^{-1}. The analysis focused on the low-wavenumber region, particularly 400–700 cm^{-1}, because it is associated with metal–oxygen lattice vibrations, including Ti–O, Ti–O–Ti, Ca–O, and Ca–O–Ti, which are characteristic of the $TiO_2/CaTiO_3$ perovskite structure. Absorption bands in the 1600–3500 cm^{-1} region were also examined to identify possible O–H groups, H–O–H vibrations, and adsorbed water molecules on the sample surface. Bands near 1300–1500 cm^{-1} were analyzed to evaluate possible carbonate or nitrate residues originating from the precursors or synthesis process. The absorption bands were assigned by comparing the measured peak positions with recent reports on $TiO_2/CaTiO_3$ and titanate-based perovskite materials.

2.4. UV–Vis Characterization and Kubelka–Munk Analysis

UV–Vis characterization was performed to evaluate the optical response of $TiO_2/CaTiO_3$. The measured spectrum was used to examine the optical-absorption behavior of the sample, particularly in the ultraviolet and visible regions. For a powdered or reflective solid sample, the reflectance data were transformed using the Kubelka–Munk function to provide an approximation of the apparent absorption coefficient. The Kubelka–Munk remission function is given in Equation (1). Where F(R) is the Kubelka–Munk remission function and R is the diffuse reflectance of the sample. The Kubelka–Munk band-gap relation used in this study is given in Equation (2).

$$F(R) = \frac{(1-R)^2}{2R} \quad (1)$$

$$[F(R)h\nu]^{\mathrm{n}} = A(h\nu - E^{\mathrm{g}}) \quad (2)$$

Where hν is the photon energy, A is a constant, E^g is the optical band gap energy, and n represents the optical-transition model. A plot of $[F(R)h\nu]^2$ versus hν was used for the direct-allowed transition, whereas $[F(R)h\nu]^{1/2}$ versus hν was used for the indirect-allowed transition. The band gap energy was obtained by extrapolating the linear portion of the curve to the energy axis. The Kubelka–Munk results were interpreted carefully because the estimated band gap can be influenced by particle scattering, the spectral baseline, and the selected linear region [4].

2.5. Band Gap Analysis Using the Tauc Plot

The band gap energy of $TiO_2/CaTiO_3$ was also analyzed using the Tauc-plot method as a comparison with the Kubelka–Munk results. This analysis evaluated the consistency of the optical band gap estimates for direct and indirect transition models. The Tauc equation is given in Equation (3) [9]. where α is the absorption coefficient, hν is the photon energy, A is a constant, E^g is the optical band gap energy, and n represents the electronic-transition model. A plot of $(\alpha h\nu)^2$ versus hν was used for the direct-allowed transition, whereas $(\alpha h\nu)^{1/2}$ versus hν was used for the indirect-allowed transition. E^g was determined from the intercept obtained by extrapolating the linear region to the energy axis.

$$(\alpha h\nu)^{\mathrm{n}} = A(h\nu - E^{\mathrm{g}}) \quad (3)$$

The linear region was selected from the absorption edge showing the most consistent increase. The Tauc-plot results were then compared with the Kubelka–Munk values to assess the stability of the optical band gap estimate. Baseline absorption must be considered in Tauc analysis because an inappropriate baseline or fitting region can produce a substantial difference in the estimated band gap [5], [6].

2.6. Urbach Energy Analysis

Urbach energy was analyzed to evaluate optical disorder and tail states near the band edge of $TiO_2/CaTiO_3$. The broadening of localized states in the sub-band-gap region can arise from crystal defects, oxygen vacancies, lattice distortion, surface disorder, and structural residues from the synthesis process. The exponential Urbach relation between the absorption coefficient and photon energy is given in Equation (4). The linearized Urbach relation is given in Equation (5).

$$\alpha = \alpha^0 exp\left(\frac{h\nu}{E_{\mathrm{u}}}\right) \quad (4)$$

$$ln\,\alpha = ln\,\alpha^0 + \frac{h\nu}{E_{\mathrm{u}}} \quad (5)$$

Where α is the absorption coefficient, α_0 is a constant, hν is the photon energy, and E_u is the Urbach energy. The reciprocal-slope relation used to obtain E_u is given in Equation (6). For diffuse-reflectance data, α can be approximated using F(R). The diffuse-reflectance form of the Urbach relation is therefore given in Equation (7).

$$E_{\mathrm{u}} = \frac{1}{slope} \quad (6)$$

$$ln\,F(R) = ln\,F(R)^0 + \frac{h\nu}{E_{\mathrm{u}}} \quad (7)$$

Urbach energy was determined from the absorption-tail region exhibiting a linear relationship between ln α or ln F(R) and photon energy. A higher E_u indicates greater optical disorder and stronger broadening of the tail states near the band edge [7].

2.7. DTA Analysis

Differential Thermal Analysis (DTA) was performed to evaluate the principal thermal events in $TiO_2/CaTiO_3$. The powdered $TiO_2/CaTiO_3$ sample was placed in the DTA sample holder and heated at a constant heating rate to the final measurement temperature. The DTA curve was used to identify thermal events associated with the release of surface species, thermal relaxation, decomposition of precursor residues, and minor structural transformations. The thermal peak temperature, T_p, was determined from the maximum or minimum of the DTA peak, depending on whether the event was exothermic or endothermic. T_p was then used to calculate the kinetic and activation thermodynamic parameters. The DTA results were interpreted together with the FTIR data to evaluate possible relationships between the thermal events and the presence of O–H groups, adsorbed H_2O, carbonates, or precursor residues on the sample surface.

2.8. Calculation of Kinetic and Activation Thermodynamic Parameters

Kinetic and activation thermodynamic parameters were calculated from the DTA peak temperature. The evaluated parameters included the activation energy, pre-exponential factor, activation enthalpy, activation Gibbs free energy, and activation entropy. The activation energy, E_a, and pre-exponential factor, A, were determined using the Kissinger equation, given in Equation (8) [10. where β is the heating rate, R is the gas constant, T_p is the peak temperature, E_a is the activation energy, and A is the pre-exponential factor. The gas constant used was R = 8.314 J mol^{-1} K^{-1}. The conventional Kissinger slope and intercept are obtained from a plot of $ln(\beta/T_p^2)$ versus $1/T_p$ using peak temperatures measured at different heating rates.

$$ln\left(\frac{\beta}{T_p^2}\right) = ln\left(\frac{AR}{E_{\mathrm{a}}}\right) - \frac{E_{\mathrm{a}}}{RT_p} \quad (8)$$

The activation enthalpy was calculated using the transition-state relationship in Equation (9).

$$\Delta H* = E_{\mathrm{a}} - RT_p \quad (9)$$

The activation Gibbs free energy was calculated using Equation (10).

$$\Delta G* = E_a + RT_p \, ln\left(\frac{K_b T_p}{hA}\right) \quad (10)$$

The activation entropy was calculated using Equation (11). Where ΔH* is the activation enthalpy, ΔG* is the activation Gibbs free energy, ΔS* is the activation entropy, K^B is the Boltzmann constant, and h is the Planck constant. The constants used were $K^B = 1.381 \times 10^{-23}$ J K^{-1} and $h = 6.626 \times 10^{-34}$ J s.

$$\Delta S* = \frac{\Delta H* - \Delta G*}{T_p} \quad (11)$$

The kinetic and thermodynamic quantities obtained in this analysis are reported as apparent activation parameters because they were calculated from the thermal event observed in the DTA curve. Accordingly, ΔH*, ΔG*, and ΔS* are not interpreted as the thermodynamic properties of final-product formation but as parameters describing the formation of the activated state during the analyzed thermal process. This interpretation follows current recommendations for thermal-kinetic analysis [8], [11].

3. RESULTS AND DISCUSSION

3.1. FTIR Characterization Results

The phase formation and optical response of $TiO_2/CaTiO_3$ were evaluated using FTIR and UV–Vis spectra to identify the characteristic metal–oxygen bonds of the perovskite and the light-absorption behavior of the material, as shown in Figure 1.

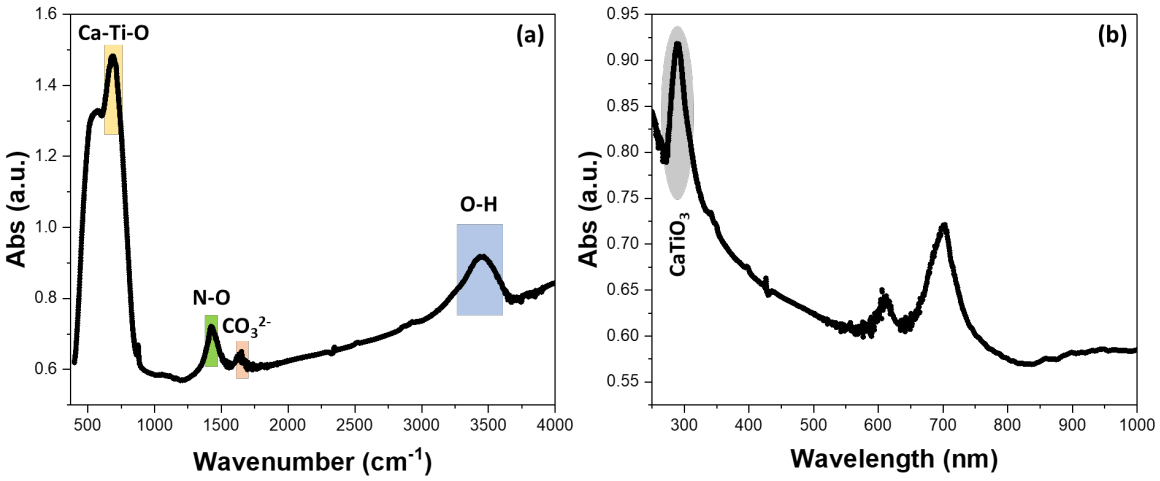

Fig. 1. Characterization results of $TiO_2/CaTiO_3$: (a) FTIR spectrum and (b) UV–Vis spectrum

Figure 1(a) shows the FTIR spectrum of $TiO_2/CaTiO_3$, with dominant absorption bands in the low-wavenumber region, particularly at approximately 400–700 cm^{-1}. This region is an important fingerprint of titanate-based perovskites because it is associated with Ti–O and Ti–O–Ti vibrations and the contribution of Ca–O bonds within the $TiO_2/CaTiO_3$ framework. The bands in this region indicate the formation of a Ca–Ti–O network rather than merely the presence of unreacted precursors. Similar Ti–O and Ti–O–Ti lattice vibrations have been reported for $TiO_2/CaTiO_3$ and related titanate perovskites [12], [13]. The assignments summarized in Table 1 further show that $TiO_2/CaTiO_3$ formation is primarily identified by metal–oxygen lattice vibrations.

Table 1. FTIR functional-group assignments for the $TiO_2/CaTiO_3$ sample

Bond	Vibrational Mode	Wavenumber (cm^{-1})	
		Data	Reference
O–H	Stretching vibration	3400–3500	~3500; 3644 [2], [13]
H–O–H / O–H	Bending vibration	1600–1650	1635–1636 [2], [13]
CO_3^{2-}	Stretching / bending vibration	1400–1500	1489 [3], [13]
NO_3^- / N–O	Stretching vibration	1380–1390	1385 [3]

Ti–O–Ti	Bridge stretching vibration	550–560	551–556; 550 [2], [12]
Ca–O–Ti / Ca–Ti–O	Stretching / bending vibration	560–565	564; 554 [12], [13]
Ti–O	Stretching vibration	430–455	442–454; 434–450 [2], [13]
Ti–O / Ca–Ti–O	Lattice vibration	450–540	450 and 540 [14]
Ti–O–Ti	Bending vibration	700	700 [3]

The bands at approximately 400–700 cm^{-1} are the most important indicators because they are directly associated with Ti–O, Ti–O–Ti, and Ca–O–Ti vibrations in the $TiO_2/CaTiO_3$ perovskite framework. Structurally, these vibrations represent interconnected TiO_6 octahedra and the role of Ca^{2+} ions in stabilizing the perovskite network. Ti–O and Ti–O–Ti bands in $TiO_2/CaTiO_3$ are commonly reported within the 430–560 cm^{-1} region, while Ca–O–Ti-related vibrations may appear at slightly higher wavenumbers [2], [12], [13]. The presence of these bands therefore indicates that the calcium and titanium sources reacted to form a calcium-titanate structure rather than remaining solely as a mixture of precursor oxides.

In addition to the principal metal–oxygen bands, Table 1 shows possible O–H and H–O–H bands at high and intermediate wavenumbers, which are generally associated with surface hydroxyl groups or adsorbed water molecules. The O–H band near 3400–3500 cm^{-1} and the H–O–H/O–H bending band near 1600–1650 cm^{-1} do not necessarily indicate a major impurity phase but more commonly represent surface moisture or hydroxyl groups bound to the particle surface [13]. The relatively lower intensity of the O–H bands compared with the Ti–O and Ti–O–Ti bands indicates that these surface species do not dominate the material structure and instead represent common surface features of oxides synthesized by wet-chemical and calcination processes.

Additional bands near 1380–1500 cm^{-1}, when present, can be associated with nitrate or carbonate residues originating from the precursors or synthesis medium. A band near 1385 cm^{-1} may be related to N–O stretching when nitric acid is used during precursor dissolution, whereas carbonate residues can remain if the calcium source does not decompose completely. These bands must be interpreted carefully because their intensity depends strongly on the synthesis, washing, drying, and calcination conditions. Weak carbonate or nitrate bands may indicate small amounts of precursor residues on the surface but do not necessarily alter the principal identity of the material [3].

3.2. UV–Vis Characterization Results

In the UV–Vis spectrum shown in Figure 1(b), $TiO_2/CaTiO_3$ exhibits stronger absorption in the ultraviolet region, which gradually decreases toward the visible region. This behavior is consistent with the wide-band-gap character of $TiO_2/CaTiO_3$. Electronically, the valence-band edge of $TiO_2/CaTiO_3$ is primarily formed by O 2p states, whereas the conduction-band edge is dominated by Ti 3d states; therefore, the principal optical transition can be associated with electron excitation from O 2p to Ti 3d states. Experimental and theoretical studies commonly place the optical band gap of $TiO_2/CaTiO_3$ in the wide-gap range, explaining its dominant ultraviolet response [15], [16].

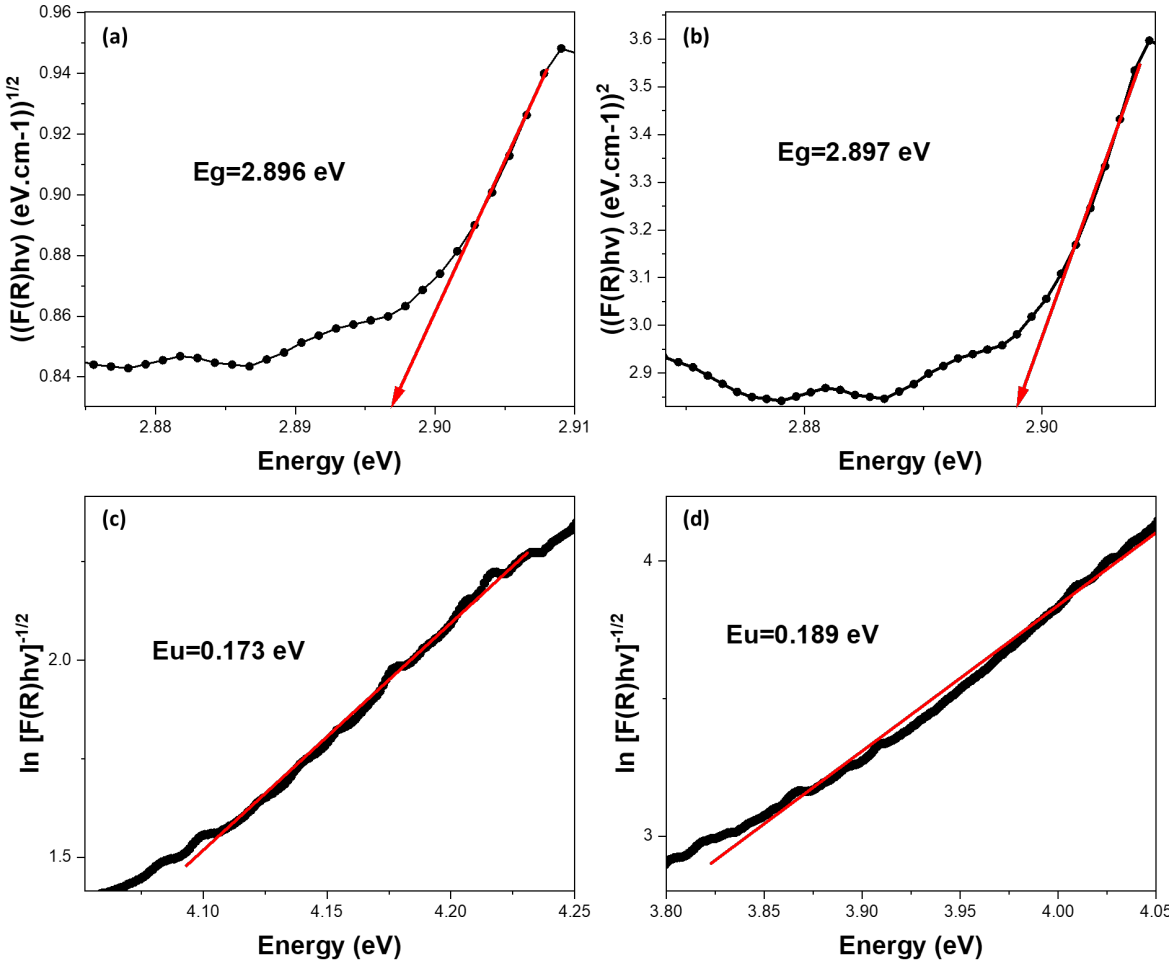

Fig. 2. Band gap and Urbach energy analysis of $TiO_2/CaTiO_3$ using the Kubelka–Munk method: (a) direct band gap, (b) indirect band gap, (c) Urbach energy derived from the direct-transition model, and (d) Urbach energy derived from the indirect-transition model

Figure 2 presents the band gap and Urbach energy analysis of $TiO_2/CaTiO_3$ based on the Kubelka–Munk transformation. Figures 2(a) and 2(b) yield direct and indirect band gap energies of 2.896 eV and 2.897 eV, respectively. The difference of only 0.001 eV indicates that the estimated absorption edge is relatively consistent for the two optical-transition models. These values place the optical response of $TiO_2/CaTiO_3$ near the UV–visible boundary, preserving its wide-gap oxide-semiconductor character while suggesting an extension of absorption toward the visible region. The optical transition in $TiO_2/CaTiO_3$ is generally associated with excitation from O 2p states in the valence band to Ti 3d states in the conduction band within the TiO_6 perovskite framework [1], [15].

The band gap of approximately 2.90 eV obtained for this sample is lower than several values reported for nominally pure $TiO_2/CaTiO_3$, which generally absorbs in the ultraviolet region. This decrease may be associated with local energy levels arising from TiO_6 octahedral distortion, oxygen vacancies, surface defects, or minor residual phases remaining after synthesis [16], [17]. Nevertheless, the nearly identical direct and indirect values should not be interpreted as proof that the two transition mechanisms are simultaneously dominant. A more cautious interpretation is that the optical absorption edge of $TiO_2/CaTiO_3$ occurs at approximately 2.90 eV, whereas the dominant transition type requires confirmation through photoluminescence, first-derivative reflectance analysis, or band-structure calculations. Such caution is necessary because Kubelka–Munk and Tauc estimates are affected by the reflectance baseline, particle scattering, and the selected linear extrapolation region [4], [5].

Figures 2(c) and 2(d) show Urbach energies of 0.173 eV for the analysis derived from the direct-band-gap model and 0.189 eV for that derived from the indirect-band-gap model. Urbach energy represents the width of localized states near the band edge and can therefore be used as an indicator of structural disorder, lattice

defects, and the distribution of sub-band-gap electronic states. The similar E_u values indicate that the optical disorder estimated from both approaches is relatively consistent. The slightly higher value of 0.189 eV suggests a greater tail-state contribution in the indirect model, although the difference is too small to indicate a substantial change in disorder. The values should nevertheless be interpreted within the known limitations of optical-tail fitting [5], [7].

To compare the band gap estimate obtained using the Kubelka–Munk approach in Figure 2, the optical analysis of $TiO_2/CaTiO_3$ was continued using the Tauc-plot method, as shown in Figure 3.

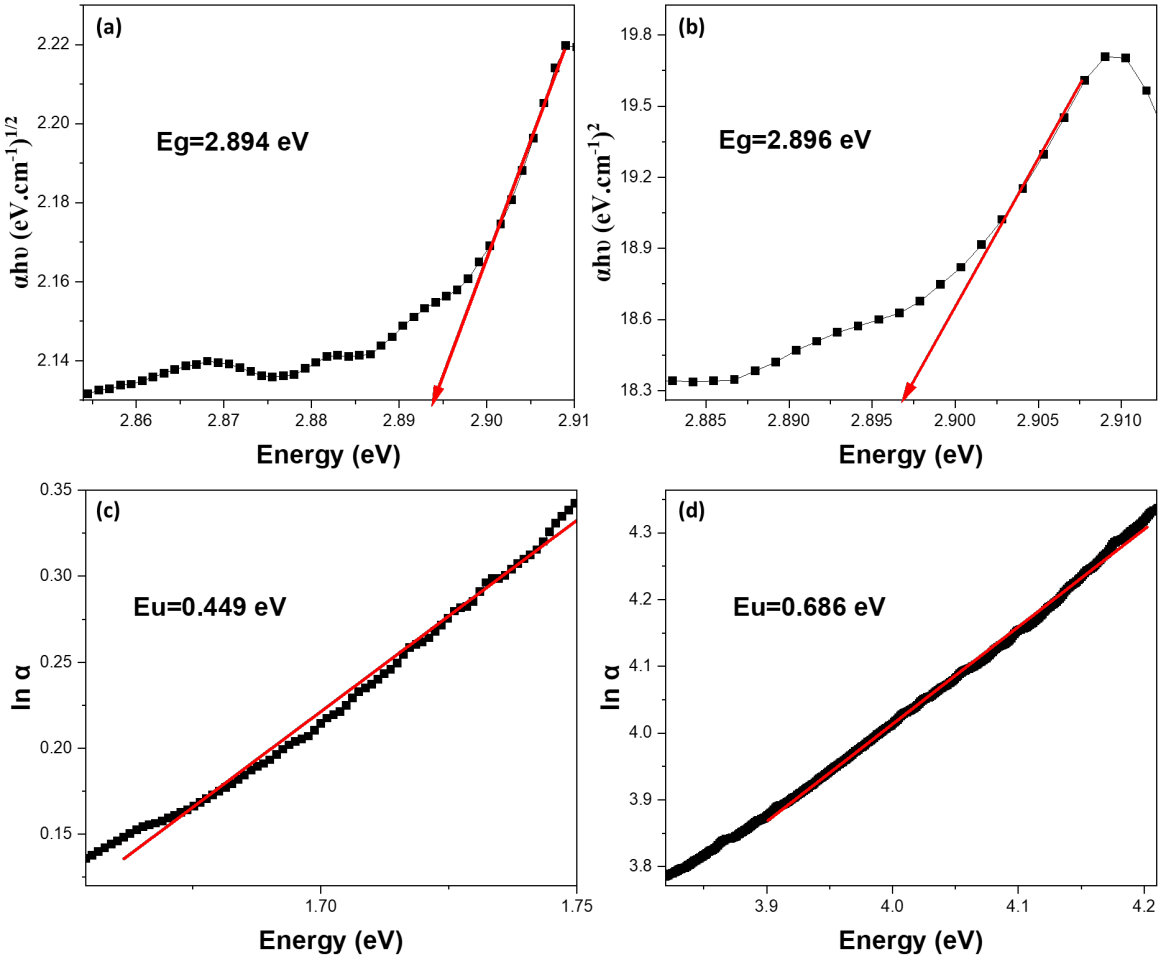

Fig. 3. Band gap and Urbach energy analysis of $TiO_2/CaTiO_3$ using the Tauc-plot method: (a) indirect band gap, (b) direct band gap, (c) Urbach energy derived from the direct-transition region, and (d) Urbach energy derived from the indirect-transition region

Figure 3 shows that the band gap energies obtained from the Tauc plots are very similar, namely 2.894 eV in panel (a) and 2.896 eV in panel (b). The close agreement indicates that the position of the optical absorption edge is relatively consistent for the two extrapolation models. These results also agree with the Kubelka–Munk analysis in Figure 2, which yielded band gap energies of approximately 2.896–2.897 eV. Thus, the optical band gap of the present $TiO_2/CaTiO_3$ sample is approximately 2.90 eV. The lower value relative to some reports for $TiO_2/CaTiO_3$ can be influenced by the synthesis conditions, calcination temperature, particle size, lattice distortion, and surface defects [1], [2].

Electronically, the reduction in the band gap of $TiO_2/CaTiO_3$ can be related to changes in the band structure involving O 2p states in the valence band and Ti 3d states in the conduction band. In oxide perovskites, local changes such as TiO_6 octahedral distortion, oxygen vacancies, and defect states can introduce additional energy levels within the band gap and shift the absorption edge toward lower energy [15], [17]. Therefore, the band gap of approximately 2.90 eV may reflect not only intrinsic band transitions in $TiO_2/CaTiO_3$ but also contributions from sub-band-gap states associated with structural or surface imperfections.

Figures 3(c) and 3(d) show Urbach energies of 0.449 eV and 0.686 eV, respectively. Urbach energy represents the width of localized states near the band edge; therefore, a higher value is generally associated with greater optical disorder, crystal defects, oxygen vacancies, or surface irregularities. The relatively high E_u values indicate pronounced tail states near the band edge of the synthesized $CaTiO_3$. However, these estimates remain sensitive to the selected spectral region and the assumptions used in the optical analysis [5], [7].

The differences between the E_u values obtained in Figures 2 and 3 must also be interpreted carefully. Band gap and Urbach energy estimates from UV–Vis or diffuse-reflectance data are strongly influenced by the original spectral profile, baseline absorption, particle scattering, and selection of the linear extrapolation region. The Kubelka–Munk transformation can be misinterpreted when its scattering and absorption assumptions are not considered, while baseline absorption in a Tauc plot can produce a substantial difference in the estimated band gap [4]–[6]. Therefore, the consistent E^g values in Figures 2 and 3 strengthen the estimated position of the optical edge, whereas the different E_u values are more appropriately understood as consequences of the sensitivity of the fitting method to the baseline and selected linear region.

The lower Urbach energy obtained from the Kubelka–Munk approach is likely more reliable for this perovskite system, particularly because the samples were analyzed from diffuse reflectance spectra where the Kubelka–Munk function provides a more direct absorption-related representation of the sub-bandgap tail. The higher values obtained from the Tauc-plot method may arise from the broader fitting window and the linearization procedure, which can incorporate contributions from band-edge transitions, defect-mediated absorption, and light-scattering effects. Therefore, the Tauc-derived Urbach energy should be interpreted as an apparent disorder parameter, whereas the Kubelka–Munk-derived values more closely reflect the localized tail states near the absorption edge.

3.3. DTA Characterization Results

In addition to the vibrational and optical evaluations, the thermal stability of $TiO_2/CaTiO_3$ was analyzed using DTA to identify the principal thermal event and derive the kinetic and activation thermodynamic parameters, as shown in Figure 4.

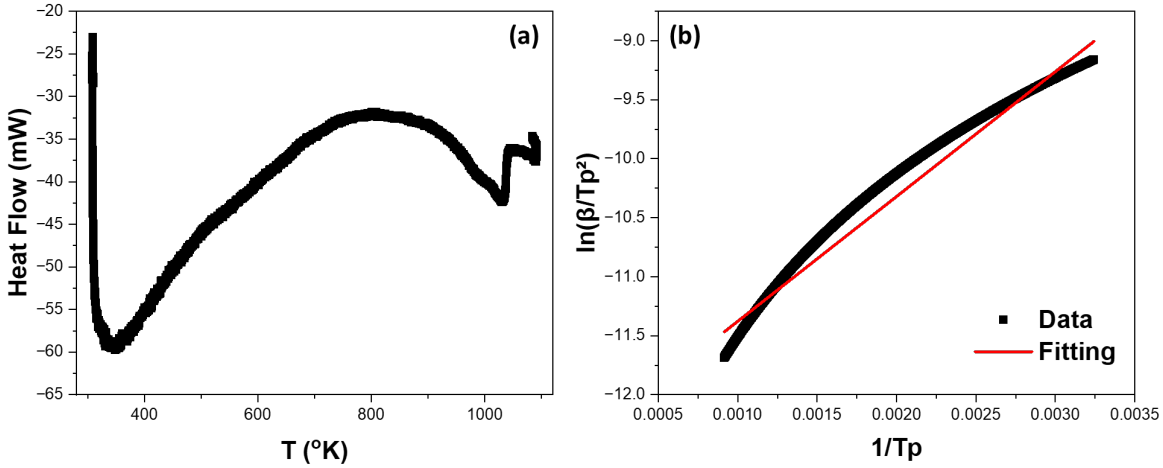

Fig. 4. DTA thermogram of $TiO_2/CaTiO_3$

Figure 4 shows the DTA thermogram of $TiO_2/CaTiO_3$ used to determine the principal thermal peak temperature of the material. The kinetic and activation thermodynamic parameters were calculated using the Kissinger and transition-state relationships defined in Equations (8)–(11). These relations provide the activation energy, pre-exponential factor, activation enthalpy, activation Gibbs free energy, and activation entropy associated with the thermal event [10]. The resulting parameters are presented in Table 2.

Table 2. Thermodynamic and kinetic parameters derived from the DTA trace

Sample	Value
Tp (K)	623.31
ΔH (kJ mol^{-1}	1.511
ΔG* (kJ mol^{-1})	233.89
ΔS (J mol^{-1} K^{-1})	-301.26
Ea (kJ mol^{-1})	7.853

ln A	-5.238

As shown in Table 2, the peak temperature, T_p, of $TiO_2/CaTiO_3$ was 623.31 K, equivalent to approximately 350.16 °C. This value indicates a thermal event in the intermediate-temperature range. For $TiO_2/CaTiO_3$, an event within this range is more appropriately interpreted as thermal relaxation, release of surface species, or a minor transformation related to residual synthesis products rather than as the principal formation of the $TiO_2/CaTiO_3$ phase. Several studies have reported that more complete $TiO_2/CaTiO_3$ formation and crystallization generally require higher thermal treatments, depending on the synthesis route and precursor system [1]–[3]. In a $TiO_2/CaTiO_3$ system derived from calcium precursors, calcination at up to 900 °C was reported to decrease mass loss and produce a more stable and crystalline structure [3].

The DTA result is also consistent with the preceding FTIR interpretation. The O–H/H_2O, carbonate, and possible nitrate bands in Table 1 suggest that the $TiO_2/CaTiO_3$ surface may retain adsorbed species or small amounts of precursor residues. Therefore, the thermal event near T_p = 623.31 K may be associated with the release or reorganization of these surface species, particularly when no other major high-temperature event is observed. Thermal studies of $TiO_2/CaTiO_3$ prepared through wet-chemical routes have similarly shown that the measured curve can contain several physicochemical events, including the release of adsorbed water before subsequent oxide transformations [2], [18].

The kinetic parameters in Table 2 show that the activation energy, E_a, of $TiO_2/CaTiO_3$ is 7.853 kJ mol^{-1}, while the activation enthalpy, ΔH*, is 1.511 kJ mol^{-1}. These relatively low values indicate that the detected thermal event does not require a large energy barrier. In other words, the change occurring near 623.31 K is unlikely to represent massive formation of the $TiO_2/CaTiO_3$ lattice and more likely reflects a low-energy process such as local lattice relaxation, release of surface groups, or decomposition of minor residues. In thermal analysis, E_a and A describe the kinetic barrier and frequency of the thermally activated process, whereas ΔH*, ΔG*, and ΔS* describe the activated state rather than the overall thermodynamics of the final reaction [8], [10], [11].

The activation Gibbs free energy, ΔG*, of 233.89 kJ mol^{-1} indicates that formation of the activated state requires thermal energy. A positive ΔG* does not mean that the overall formation of $TiO_2/CaTiO_3$ is nonspontaneous; instead, it represents the energy barrier for forming the transition state of the analyzed thermal event. This distinction is important because ΔG* in thermal-kinetic analysis refers to activation Gibbs free energy and must not be equated with the Gibbs free energy of the complete product-forming reaction [8]. The activation entropy, ΔS*, of −301.26 J mol^{-1} K^{-1} indicates that the transition state is more ordered than the initial state. This negative value may be associated with restricted degrees of freedom during the thermal process, for example through reorganization of surface species, interparticle interactions, or formation of a more ordered intermediate configuration before the event occurs. Negative ΔS* values generally indicate that formation of the activated complex involves a decrease in degrees of freedom or an increase in system order. The value of ln A = −5.238 also indicates a relatively low pre-exponential factor in the kinetic model, suggesting a low frequency of effective activation events [8].

4. CONCLUSION

The integrated FTIR, UV–Vis, and DTA analyses provide a coherent description of the vibrational, optical, and thermal characteristics of $TiO_2/CaTiO_3$. The FTIR spectrum showed the characteristic Ti–O, Ti–O–Ti, and Ca–O–Ti lattice vibrations associated with the $TiO_2/CaTiO_3$ perovskite framework, together with weaker contributions from surface hydroxyl groups and residual carbonate or nitrate species. The optical absorption edge was consistently estimated at approximately 2.90 eV. The Kubelka–Munk analysis yielded direct and indirect band gap energies of 2.896 and 2.897 eV, respectively, while the Tauc-plot analysis produced corresponding values of 2.896 and 2.894 eV. In contrast, the Urbach energy was more sensitive to the analytical approach, ranging from 0.173–0.189 eV for the Kubelka–Munk treatment and 0.449–0.686 eV for the Tauc-based treatment, indicating that the estimation of tail states is strongly influenced by baseline selection and the fitted spectral region. The DTA trace exhibited a principal thermal event at 623.31 K, with apparent activation parameters of E_a = 7.853 kJ mol^{-1}, ΔH* = 1.511 kJ mol^{-1}, ΔG* = 233.89 kJ mol^{-1}, ΔS* = −301.26 J mol^{-1} K^{-1}, and ln A = −5.238. The relatively low activation barrier supports assigning this event to thermal relaxation or the release and reorganization of residual surface species rather than to bulk $TiO_2/CaTiO_3$ formation. Finally, the defect-related optical tail states, as reflected by the Urbach energy values, may influence charge-carrier recombination, light absorption, and optical sensitivity. Therefore, controlling these localized states, together with the observed thermal stability, is important for improving the potential performance of $TiO_2/CaTiO_3$-based materials in solar cells, photodetectors, optical sensors, and photocatalytic systems requiring stable operation under elevated-temperature conditions.

Acknowledgments

The authors acknowledge that the experimental dataset analyzed in this article was generated in the study previously published by Kurniawidi et al. [3]. This research was funded by the 2023 fiscal year Internal Fund Grant of the University of Mataram through the Senior Lecturer Acceleration Research Scheme under contract number 2536/UN18.L1/PP/2024 in the name of Dian W. Kurniawidi.

Author Contributions

Kormil Saputra: Conceptualization, Methodology, Formal analysis, Investigation, Data curation, Writing - Original Draft, Visualization; Dian Wijaya Kurniawidi: Validation, Resources, Writing - Review & Editing, Supervision, Project administration, Funding acquisition; Aws Maseer Nejres: Methodology, Formal analysis, Validation, Writing - Review & Editing, Resources.

Funding

This research was funded by the 2023 fiscal year Internal Fund Grant of the University of Mataram through the Senior Lecturer Acceleration Research Scheme under contract number 2536/UN18.L1/PP/2024 in the name of Dian W. Kurniawidi.

REFERENCES

[1] L. Cerón-Urbano, C. J. Aguilar, J. E. Diosa, and E. Mosquera-Vargas, "Nanoparticles of the perovskite-structure $CaTiO_3$ system: The synthesis, characterization, and evaluation of its photocatalytic capacity to degrade emerging pollutants," Nanomaterials, vol. 13, no. 22, Art. no. 2967, 2023, doi: 10.3390/nano13222967.

[2] S. Mishra, P. K. Naini, and B. Sundaram, "Effect of calcination temperature on structural, optical and photocatalytic properties of calcium titanate ($CaTiO_3$) nanoparticle," Results in Optics, vol. 16, Art. no. 100676, 2024, doi: 10.1016/j.rio.2024.100676.

[3] D. W. Kurniawidi, S. Rahayu, A. Budianto, K. Saputra, W. P. Agista, T. Suprayogi, and R. Marlina, "Synthesis and characterization of $TiO_2/CaTiO_3$ perovskite composite derived from Pinctada maxima shell waste," Science and Technology Indonesia, vol. 10, no. 3, pp. 924–942, 2025, doi: 10.26554/sti.2025.10.3.924-942.

[4] S. Landi Jr., I. R. Segundo, E. Freitas, M. Vasilevskiy, J. Carneiro, and C. J. Tavares, "Use and misuse of the Kubelka–Munk function to obtain the band gap energy from diffuse reflectance measurements," Solid State Communications, vol. 341, Art. no. 114573, 2022, doi: 10.1016/j.ssc.2021.114573.

[5] J. Klein, L. Kampermann, B. Mockenhaupt, M. Behrens, J. Strunk, and G. Bacher, "Limitations of the Tauc plot method," Advanced Functional Materials, vol. 33, no. 47, Art. no. 2304523, 2023, doi: 10.1002/adfm.202304523.

[6] H. Zhong et al., "Idealizing Tauc plot for accurate bandgap determination of semiconductor with ultraviolet–visible spectroscopy: A case study for cubic boron arsenide," Journal of Physical Chemistry Letters, vol. 14, no. 29, pp. 6702–6708, 2023, doi: 10.1021/acs.jpclett.3c01416.

[7] F. Urbach, "The long-wavelength edge of photographic sensitivity and of the electronic absorption of solids," Physical Review, vol. 92, no. 5, p. 1324, 1953, doi: 10.1103/PhysRev.92.1324.

[8] S. Vyazovkin, "Misinterpretation of thermodynamic parameters evaluated from activation energy and preexponential factor determined in thermal analysis experiments," Thermo, vol. 4, no. 3, pp. 373–381, 2024, doi: 10.3390/thermo4030019.

[9] J. Tauc, R. Grigorovici, and A. Vancu, "Optical properties and electronic structure of amorphous germanium," Physica Status Solidi (b), vol. 15, no. 2, pp. 627–637, 1966, doi: 10.1002/pssb.19660150224.

[10] H. E. Kissinger, "Reaction kinetics in differential thermal analysis," Analytical Chemistry, vol. 29, no. 11, pp. 1702–1706, 1957, doi: 10.1021/ac60131a045.

[11] S. Vyazovkin et al., "ICTAC Kinetics Committee recommendations for performing kinetic computations on thermal analysis data," Thermochimica Acta, vol. 520, nos. 1–2, pp. 1–19, 2011, doi: 10.1016/j.tca.2011.03.034.

[12] K. Mužina, M. Tkalčević, F. Brleković, I. K. Munda, V. Mandić, J. Šipušić, and S. Kurajica, "Sol-gel synthesis and characterization of lithium and cerium codoped perovskite," Journal of Materials and Applications, vol. 9, no. 1, pp. 17–24, 2020, doi: 10.32732/jma.2020.9.1.17.

[13] M. F. García-Mendoza et al., "$CaTiO_3$ perovskite synthetized by chemical route at low temperatures for application as a photocatalyst for the degradation of methylene blue," Journal of Materials Science: Materials in Electronics, vol. 34, Art. no. 873, 2023, doi: 10.1007/s10854-023-10309-w.
[14] D. Parajuli, N. Murali, K. Samatha, N. L. Shah, and B. R. Sharma, "Structural, morphological, and textural properties of coprecipitated $CaTiO_3$ for anion exchange in the electrolyzer," Journal of Nepal Physical Society, vol. 9, no. 1, pp. 137–142, 2023, doi: 10.3126/jnphyssoc.v9i1.57751.
[15] X. Guo, Y. Li, W. Xiao, and H. Wu, "First-principles study on the electronic structure and optical properties of orthorhombic $CaTiO_3$ under different pressures," Physica C: Superconductivity and its Applications, vol. 617, Art. no. 1354447, 2024, doi: 10.1016/j.physc.2024.1354447.
[16] H. Bantawal, U. S. Shenoy, and D. K. Bhat, "Vanadium doped $CaTiO_3$ cuboids: Role of vanadium in improving the photocatalytic activity," Nanoscale Advances, vol. 3, pp. 5301–5311, 2021, doi: 10.1039/D1NA00468A.
[17] J. Li et al., "Quenching-induced oxygen vacancy engineering boosts photocatalytic activities of $CaTiO_3$," Applied Surface Science, vol. 670, Art. no. 160619, 2024, doi: 10.1016/j.apsusc.2024.160619.
[18] S. A. U. Portia et al., "Effect of annealing temperature on structural, optical and visible light photocatalytic performance of $CaTiO_3$ catalysts synthesized by simple sol-gel technique," Inorganic Chemistry Communications, vol. 119, Art. no. 108051, 2020, doi: 10.1016/j.inoche.2020.108051.